ADVANCED FUNCTIONAL MATERIALS
www.afm-journal.de

Ladder-Type Benzene-Perylene Dyes with Efficient Laser Properties in the Near-IR by Detracting/Activating Low/High Frequency Vibronic Modes

Marcos Díaz-Fernández, Álex Farrando Pérez, Fernando Gordillo Gámez, Pedro G. Boj, José M. Villalvilla, José A. Quintana, Yanpei Wan, Daniel Aranda, José Manuel Marín-Beloqui, Jishan Wu, Zebing Zeng,* María A. Díaz-García,* and Juan Casado**

Organic lasers are very attractive light sources for various applications, which have propelled the search for organic compounds showing good performance as active laser units. Here, a family of ladder-type oligomers (named as NNR-n with n = 1–4), constructed by benzene and perylene is presented. These molecules show outstanding amplified spontaneous emission properties in terms of threshold and photostability, being particularly noticeably the larger size molecules emitting in the near infrared (NIR) region. The origin of this behavior is elucidated through comprehensive spectroscopic and theoretical characterization investigating the underlying photophysical processes using steady-state absorption and emission measurements at both room temperature and cryogenic conditions, complemented by transient absorption spectroscopy spanning the visible to near-infrared (vis-NIR) regions. The results demonstrate that the excited-state electronic dynamics are governed by high-frequency vibrational modes. The rigid ladder-type structure suppresses low-frequency vibronic coupling modes, thereby significantly reducing internal conversion, which enhances NIR emission by promoting efficient radiative pathways. Finally, distributed feedback lasers have been made to exploit such optical properties resulting in devices with lasing up to 758 nm.

1. Introduction

Photophysical properties of benzene-based polycyclic compounds are of permanent interest due, among other reasons, to the presence of light absorption and emission bands in the visible spectral region thus providing a unique platform for "chromophoric" applications.[1–3] Benzenoid organic molecules can be divided in several classes (**Scheme 1**), namely: i) benzene fused systems such as polycyclic aromatic compounds or nanographenes,[4] including acenes;[5] ii) benzene oligomers or oligophenyls[6] in which the repeating phenyl rings are connected by CC single bonds; iii) fluorene and oligofluorenes,[7] in which the biphenyl repeating unit is conformationally fixed to be planar by the inclusion of two CC single bonds through the benzene ortho positions in the monomeric units (i.e., keeping the intermonomer connections with CC single bonds); and iv) ladder-type oligophenyls

M. Díaz-Fernández, F. Gordillo Gámez, D. Aranda, J. M. Marín-Beloqui, J. Casado
Department of Physical Chemistry
University of Málaga
Andalucía Tech.
Campus de Teatinos s/n
Malaga 29071, Spain
E-mail: casado@uma.es

The ORCID identification number(s) for the author(s) of this article can be found under https://doi.org/10.1002/adfm.202506356

DOI: 10.1002/adfm.202506356

Á. F. Pérez, J. M. Villalvilla, M. A. Díaz-García
Departamento Física Aplicada and Instituto Universitario de Materiales de Alicante
Universidad de Alicante
Alicante 03080, Spain
E-mail: maria.diaz@ua.es

P. G. Boj, J. A. Quintana
Departamento Óptica
Farmacología y Anatomía and Instituto Universitario de Materiales de Alicante
Universidad de Alicante
Alicante 03080, Spain

Y. Wan, Z. Zeng
State Key Laboratory of Chemo and Biosensing
College of Chemistry and Chemical Engineering
Hunan University
Changsha 410082, China
E-mail: zbzeng@hnu.edu.cn

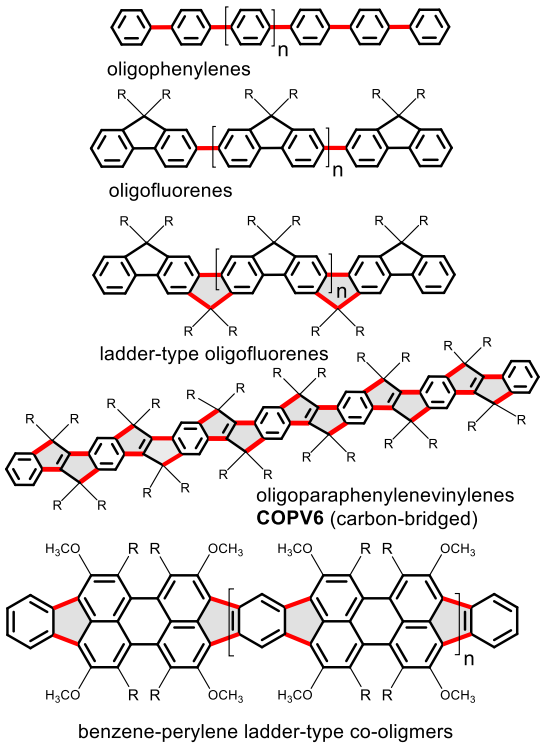

Scheme 1. Chemical structures of the typical benzene-based oligomers with different interunit connectivities (highlighted in red and grey) and **NNR-n** compounds under study. R: alkyl/phenyl solubilizing groups.

or oligofluorenes,[8] in which the rigidity through CC single bonds like fluorene is extended among all pairs of consecutive benzene rings of the molecule. To diversify the optoelectronic properties, benzene-based oligomers have been also prepared by mixing different aromatic units, conforming the so-called hetero-oligomers (i.e., in contrast to homo-oligomers with equal repeating units). A relevant example of hetero-oligomers are those with alternating benzene and fluorene moieties, and these functionalized with donor and acceptor groups, which have been exploited in a variety of applications in organic electronics, such as organic light emitting diodes,[9] organic field effect transistors,[10] electron transfer systems for organic photovoltaics,[11] sensors,[12] organic lasers,[13] etc.

An aspect that has received recently great interest in the area of organic chromophores concerns the attainment of optical absorption and emission of light in the near infrared (NIR) region of the electromagnetic spectrum. Many potential benefits of NIR

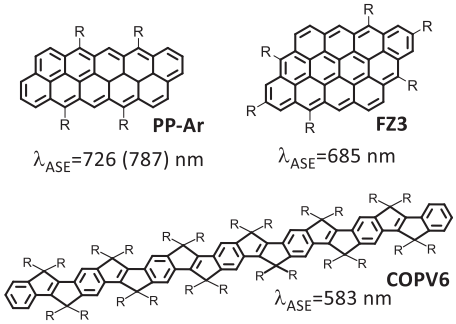

Scheme 2. Chemical structures of the main chromophores in which amplification of light emission is reported, and DFB laser is fabricated. R: alkyl/phenyl solubilizing groups.

photonic applications are in the field of energy storage with fluorescence up-conversion, analysis of biological tissues with bioimaging, etc.[14,15] In this regard, nanographenes have appeared as promising candidates in NIR applications, given that their optical gaps can be efficiently narrowed by elongating the planar molecular fragment in 2D dimensions (i.e., **PP-Ar** and **FZ3** in Scheme 1).[16,17] This strategy is however, limited by the solubility and processability of the flat $\pi-\pi$ interacting systems. Furthermore, the use of oligomeric compounds (more processable oligophenyls and oligofluorenes) for NIR optical applications appears also limited by the quick saturation of the optical (i.e., ≈500–550 nm) and HOMO-LUMO gaps with the chain length (i.e., coalescence of the mean conjugation length).[18] Finally, the last adverse situation in order to manipulate light emission in the NIR region with organic chromophores consists with the increasing efficiency of non-radiative processes (band gap law), which all work to quench emission.[19] In this scenario, the class of ladder-type oligomers, in which backbone rigidity is imposed in the interbenzene connections to block conformations, is effective to mitigate non-radiative quenching. This is the case for fluorene and ladder-type oligofluorenes and, more recently in our group, carbon-bridged oligophenylenevinylenes[20–22] (**COPV6** in Scheme 1 as the prototypical example). In this latter family, outstanding emission and lasing behavior was discovered, although the optical emission range is limited to 600 nm far from the NIR part of interest.

Another alternatives to achieve laser performance toward the NIR region, assessed through amplified spontaneous emission (ASE) studies, have been reported, such as: i) by means of excited-state intramolecular proton transfer (ESIPT) which enabled multicolor ASE extending up to 900 nm when incorporating these molecules into polystyrene (PS) microspheres;[23–25] and ii) by incorporation of heteroatom-containing units into the organic framework.[26,27] Nonetheless, extending conjugation is the most recurrent approach to get NIR ASE emitters, and **Scheme 2** shows the nanographene extending conjugation approaches investigated by our groups in which ASE was successfully found in the NIR region.[16,17]

Another important aspect of organic chromophores displaying ASE is the viable implementation in the construction of distributed feedback (DFB) lasers with very narrow (<1 nm) single-mode emissions. A particular device architecture which offers various advantages is including a laser resonator made of

J. Wu
Department of Chemistry
National University of Singapore
3 Science Drive 3, Singapore 117543, Singapore
E-mail: chmwuj@nus.edu.sg
J. Casado
Instituto Universitario de Investigación de Nanomateriales y Tecnología (IMANA) de la Universidad de Málaga
Malaga, Spain

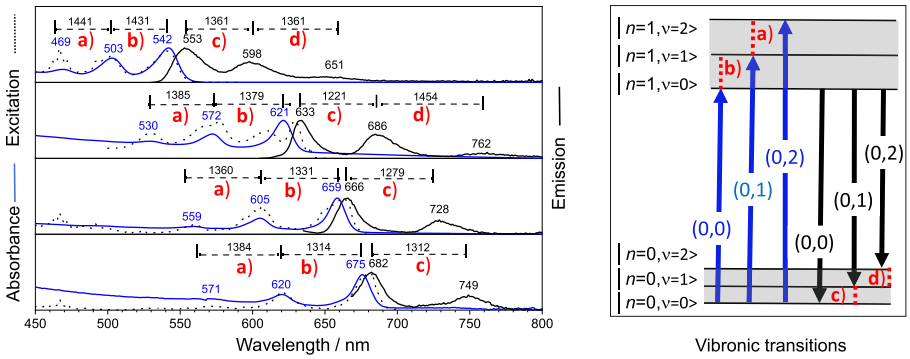

Figure 1. Left: Absorption and emission spectra of **NNR-n** in methyl THF at 80 K (10^{-5} M), from the top to the bottom: **NNR-1**, **NNR-2, NNR-3** and **NNR-4**. Right: Vibrational structure of the ground electronic (S_0) state and of the first singlet optically active excited state (S_0) according with the vibronic structure of the $S_0 \rightarrow S_1$ absorption and of the $S_1 \rightarrow S_0$ emission.

dichromated gelatin (DCG) with an engraved surface relief grating fabricated by holographic lithography (HL) and located on top of the active film.[28–30] For instance, i) the optical properties of the active film remain preserved thanks to the deposition of the DCG layer from a water solution, avoiding the use of organic solvents that can damage the film; and ii) the versatility of HL and the uniform thickness of the active film (h) enable the realization of devices emitting at different wavelengths while maintaining the respective low thresholds, enhancing overall device performance. The good laser tuning characteristics exhibited by the devices fabricated arise from their considerable size (i.e., centimetres), the versatility facilitated by HL method, and the constant value of h maintained across the entire device.

In this article, we propose to use new hetero-oligomers with ladder-type connections based on benzene and perylene as alternating repeating units of increasing molecular size (compounds named as **NNR-n** with n = 1–4, see Scheme 1), which shows light emission in the NIR region.[31] The dual combination of ladder-type and hetero-oligomeric functionality is effective to partially overcome the limiting factor of optical gap saturation of 1D oligomers thus reaching the NIR optical gaps, at the same time that restricts the adverse emission quenching effects by deactivation of low frequency vibrational modes to the point of obtaining outstanding yields of NIR fluorescence emission. Herein, a complete photophysical study at 298 and 80 K, including steady-state and time-resolved spectroscopies, is carried out in conjunction with quantum chemical calculations. Besides, a complete characterization of the ASE properties of the **NNR-n** oligomers dispersed in polystyrene (PS) films is performed to assess their potential as active materials for NIR laser purposes. Finally, the work is culminated with the fabrication of all-solution-processed DFB lasers with top-layer DCG resonators.

2. Experimental Results

2.1. Absorption and Emission Properties

Figure 1 displays the absorption and emission spectra of the four compounds at 80 K in methyl-THF (results at higher temperatures are shown in Figure S1, Supporting Information). For **NNR-1**, the absorption spectrum displays a lowest energy electronic band owing to the HOMO-LUMO one-electron excitation, which is composed of three well-resolved contributions pertaining to the 0-0, 0-1, and 0-2 vibronic transitions with the 0-0 one being the most intense. These vibronic absorption bands get more resolved upon cooling at 80 K and their vibronic spacings can be easily measured as 1431 cm^{-1} [$\nu_{01/00} = \nu(0\text{-}1) - \nu(0\text{-}0)$] and 1441 cm^{-1} [$\nu_{02/01} = \nu(\nu(0\text{-}2) - \nu(0\text{-}1)$] resulting in a sole vibronic progression or two of very similar high frequency. This is uncommon as the typical organic chromophores display vibronic structures accounted by different vibronic wavenumber progressions revealing different vibrational states coupled to the electronic transition. This dominant 1440–1430 cm^{-1} vibronic progression can be related to the existence of several intense Raman bands in the same region ≈1400 cm^{-1} (see Figure S2, Supporting Information). By increasing the length of the oligomers, the same situation is observed, where one sole vibronic progression dictates the form of the spectra 1379/1385 cm^{-1} in **NNR-2**, 1331/1360 cm^{-1} in **NNR-3** and 1314/1384 cm^{-1} in **NNR-4**. The existence of one or several similar vibronic progressions, all of them associated with high frequency vibrational states, can be explained by the effective conformational rigidity.

As for the photoluminescence (PL), the emission spectrum of **NNR-1** is broad and, contrarily to its parent absorption, vibronically unresolved at 298 K, while, upon cooling, it becomes greatly resolved giving rise to three distinctive vibronic components due to the 0-0, 0-1, and 0-2 transitions in decreasing order of energy which are equally spaced by $\nu_{00/01} = \nu_{01/02} = 1361$ cm^{-1} as a result of the activation of one or two (i.e., with very similar frequency) vibronic progressions such as in the absorptions. A similar description is valid for **NNR-2**, with the new finding that a third vibronic peak in the emission spectrum (762 nm), which is not observed at 298 K, gets resolved at 80 K. The vibronic spacings between the three peaks are $\nu_{00/01} = 1221$ cm^{-1} and $\nu_{01/02} = 1454$ cm^{-1}, revealing that, again, the two vibrational progressions involved in the electronic transition are relatively high-frequency modes, though not identical, such as in **NNR-1** (i.e., 1361 cm^{-1}).

Quantum chemical calculations with DFT and TD-DFT using the Gaussian 16[32] code with the CAM-B3LYP functional[33] and 6-31G** basis set[34,35] have been carried out. In order to support the assignments of the experimental electronic absorption and emission spectra, vibronic calculations were performed with the FCclasses3 code,[36] utilizing the Vertical Hessian Model[37] in internal coordinates[38] to account for frequency changes on the

excited states and radiative rate constants.[39,40] Figure S3 (Supporting Information) compares these experimental and theoretical electronic spectra both including their vibronic progressions (i.e., in the theoretical cases, dimensionless normal coordinates displacement parameters -ΔQ_i- in Table S1 (Supporting Information), simulate the vibronic activity), revealing a nice agreement between theory and experiments. It is observed (Table S1, Supporting Information) that the low energy vibronic modes in general reduce their activity on enlarging the $\pi-$conjugated system (modes at 70-210 cm^{-1} for **NNR-1** with larger ΔQ_i (0.85–1.16) evolve at only one relevant mode at 19 cm^{-1} in **NNR-2** and 70 cm^{-1} in **NNR-3** with an even smaller ΔQ_i of 0.70, see motion animations for some selected vibrational modes in the additional Supporting Information files). This means that for these soft vibronic modes, the higher ΔQ_i values become more localized for the frequencies below 70 cm^{-1} on going from **NNR-1→NNR-3**. Conversely, the high energy modes (1200–1500 cm^{-1}) turn out to be the most active (ΔQ_i ranging in the 0.66–0.76 interval for the three compounds), then undergoing no major changes with molecular size. This theoretical prediction seemingly indicates the activation in the vibronic progressions of high frequency modes at the expense of the softer vibronic modes, which might be the result of the ladder-type structure of the **NNR-n** compounds.

Going back to the experimental spectra and comparing the absorptions and emissions, the wavenumber of the $\nu_{00/01}$ in absorption of **NNR-2** (i.e., 1379 cm^{-1}) is higher than the $\nu_{00/01}$ in emission (i.e., 1221 cm^{-1}). However, this trend is reversed in the second vibronic component, where the absorption wavenumber (i.e., 1385 cm^{-1}) is smaller than the corresponding emission wavenumber $\nu_{01/02}$ (i.e., 1454 cm^{-1}). In the **NNR-3**, the emission spectrum at 80 K has two vibronic bands only (due to the instrument detection limit), therefore, only one vibronic progression is measured (i.e., 1279 cm^{-1}), which is smaller than the equivalent component in the absorption (i.e., 1331 cm^{-1}) such as in **NNR-1** and in **NNR-2**. In **NNR-4**, again, only two vibronic bands are detected in the emission spectrum resulting in a vibronic progression wavenumber of 1312 $cm^{-1,}$ which is now very similar to the same progression in absorption, 1314 cm^{-1}. This comparison between the absorption and emission behavior reveals three important aspects:

i. In the first vibronic progression of the emission, the wavenumber increases from **NNR-2** (1221 cm^{-1}) to **NNR-3** (1279 cm^{-1}) and to **NNR-4** (1312 cm^{-1}).
ii. Increasing the molecular size produces a convergence of the absorption and emission vibronic progressions to the same values, such as in **NNR-4**.
iii. Vibrational spacings are larger in the optically active excited state (i.e., S_1 obtained from the absorption spectra) than in the ground electronic state (i.e., S_0 obtained from the emission spectra), which is unusual since the less overall bonding character of excited states compared with the ground state. This situation has been previously described for benzene and some of its derivatives[41,42] a phenomenon ascribed to the presence of a particular vibrational coordinate, the so-called kékulé CC stretching mode of benzene, which couples the excitation between the S_0 and S_1 and whose force constant increases in the excited state. This arises because alongside this vibronically coupling kékulé CC stretching mode, the excited state shows a greater potential energy slope than in the ground state, revealing the existence of an excited state stiffening effect that, in our **NNR-n** molecules, could be associated with the presence of ortho-substituted benzenes in analogy with this effect being found previously in benzene and ortho-disubstituted benzenes. On the other hand, the stokes shift (i.e., difference between the 0-0 vibronic peaks in absorbance and in emission) in the four compounds progressively decreases upon increment of the number of repeating units and, at 80 K, it is almost vanishing in **NNR-4** (i.e., 152 cm^{-1}). This is in agreement with the increase of the fluorescence quantum yields (Φ_F) from **NNR-1→NNR-3/NNR-4** which is a very important property with a dual origin; on one hand, the same behavior has been found out in oligophenyls where Φ_F increases with increasing length ascribed to the decrease of the intersystem crossing rate resulting in reduced interference with fluorescence with the increase of the molecular size.[43] The lifetimes for the fluorescence emissions slightly decrease as **NNR-1** (3.23 ns)→ **NNR-2** (2.97 ns) → **NNR-3** (2.07 ns) → **NNR-4** (2.11 ns) in agreement with the increase of Φ_F. On the other hand, the most unique aspect of the studied compounds is related to the ladder-type structure which blocks conformational flexibility and reduces the stokes shift. Aside of pure electronic effect and taking into the experimental low temperature vibronic progressions in absorption and emission together with theoretical calculations of the vibronic progressions, it turns out that the particular ladder-type structure removes the low frequency vibrational modes from the electronic excitations. These vibrational modes represent efficient channels of emission quenching and thus their absence in the **NNR-n** compounds promotes the increment of Φ_F with size (i.e., this will be very valuable for attaining ASE in the vicinity of the NIR region).

2.2. Femtosecond Transient Absorption Spectroscopy (fs-TAS)

Fs-TA spectra of the four compounds have been obtained. They were excited with the same power (0.25 mW) at their absorbance maxima, at 540, 620, 660, and 680 nm for **NNR-1**, **NNR-2**, **NNR-3**, and **NNR-4**, respectively. **Figure 2** shows the fs-TAS spectra of the four **NNR-n** obtained at certain time delays upon population of the first optically active excited state, by the pump pulse. The main aspects of these data are: i) a positive feature corresponding to the excited state absorbance or ESA band spreading mostly in IR range accompanied by two negative features in the visible region owing either to the ground state bleaching (GSB) or to stimulated emission (SE) given the resemblance with the ground state absorbance and fluorescence spectra, respectively. However, since the almost negligible Stoke shifts of these molecules, the maximum of the ground state bleach and the stimulated emission almost merged together in the form of a very intense negative signal at ≈550, 625, 670, and 680 nm, for **NNR-1**, **NNR-2**, **NNR-3**, and **NNR-4**, respectively. We extract the lifetimes from the stimulated emission 0-1 vibronic band (i.e., despite this 0-1 most intense emission SE band might have contribution from the GSB). These lifetimes were 4 ns in **NNR-1**, 2 ns in **NNR-2**,

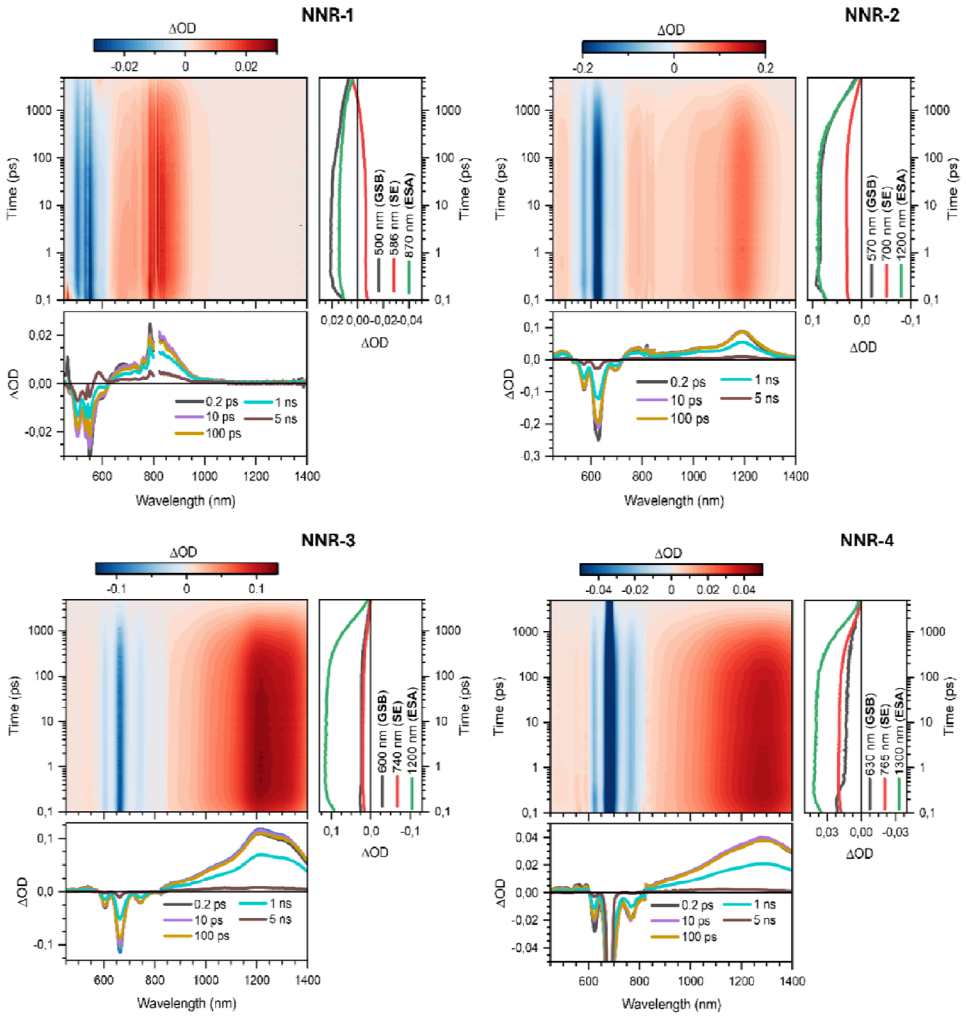

Figure 2. Fs-TA spectra of a) NNR-1, b) NNR-2, c) NNR-3, and d) NNR-4 solutions in toluene. Excitation wavelength was modified to match their 0-0 maximum absorbance. Excitation power was 0.25 mW.

1.5 ns in **NNR-3**, and 1 ns in **NNR-4**, which show the same decreasing behavior with the enlargement of the chain length than the fluorescence lifetimes obtained by the single photon counting experiments. From quantum chemical calculations, we have been able to obtain the theoretical kinetic constants for the radiative (k_r) and non-radiative (i.e., K_{IC}, internal conversion only) relaxation processes (Table S2, Supporting Information). The k_r theoretical values increase by increasing the π−conjugated size as they evolve as 1.41 10^8 s^{-1} in **NNR-1**, 3.47 10^8 s^{-1} in **NNR-2** and 5.17 10^8 s^{-1} in **NNR-3** in line with the decrease of their fluorescence lifetimes on **NNR-1**→ **NNR-4** from steady-state and transient measurements. Concomitantly, the k_{IC} theoretical values decrease from 0.87 10^8 s^{-1} in **NNR-2** to 0.23 10^8 s^{-1} in **NNR-3** (0.0083 10^8 s^{-1} in **NNR-1**), revealing the impediment for internal conversion between vibronic states upon removing the vibronic activity of soft frequency modes. On the other hand, the increase of fluorescence efficiency also reveals the decrease of the competing relaxation channels.

It turns out that the lifetimes of the stimulated emission are of the same order of magnitude than those of the spontaneous emissions, an uncommon result given that stimulated emission is conventionally detected in fs-TAS experiments of organic materials with picosecond timescale.[44–46] This delayed stimulated emission in our dyes can also be associated with the effects mentioned above to account for the larger fluorescence quantum yields.

The excited state stiffening (i.e., the higher frequency vibronic progressions) together with the absence of low frequency quenching modes provide a smaller density of states, which hampers non-radiative decays. In addition, the similar values of stimulated and spontaneous emission lifetimes are good indications of ASE, as reported in the literature.[24,47–49] The ASE properties of the compounds will be analyzed in the following sections. The main ESA bands of these benzene-perylene ladder-type oligomers are placed in the NIR region, so well separated from the SE bands avoiding interference of the two, a fact which is more marked for **NNR-3** and **NNR-4**. The state population from the ESA bands remains constant until it decays following the same kinetics as the GSB and the SE, then associated with the optically active singlet excited state described for **NNR-1/4**.

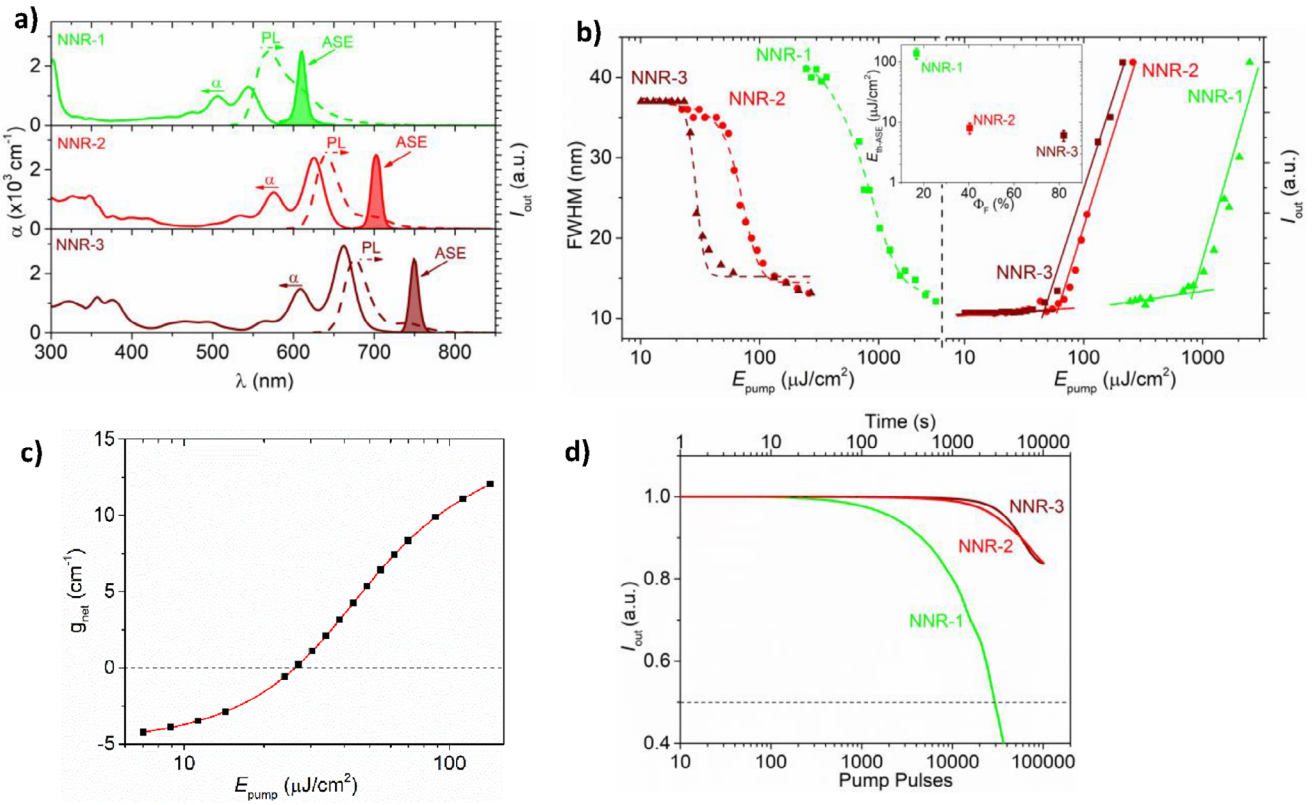

Figure 3. Optical properties of investigated NNRs dispersed in polystyrene films. a) Absorption coefficient (α; solid lines, left axis), PL (dashed lines, right axis), and ASE (shaded area, right axis) spectra at room temperature of PS films doped with 1 wt.% of **NNR-1** (top panel, green), **NNR-2** (middle panel, red), and **NNR-3** (bottom panel, maroon). b) Emission output intensity (I_{out}; right axis) and linewidth, defined as the FWHM (left axis) as a function of the pump energy density (E_{pump}) for PS films doped with 1 wt.% of **NNR-1** (green triangles), **NNR-2** (red circles), and **NNR-3** (maroon squares). Lines are guides to the eye. Inset: ASE threshold ($E_{th\text{-}ASE}$) versus fluorescence quantum efficiency in solution, Φ_F, for each NNR. Φ_F data correspond to previously reported values.[26] c) Net gain coefficients, g_{net}, versus the pump energy density, E_{pump}, for a 1 wt.% **NNR-3**-doped PS film. The full line is a guide to the eye and its intersection with the y-axis corresponds to the loss coefficient ($k = 4.3\,cm^{-1}$). d) ASE intensity, I_{out}^{ASE}, versus time, and versus the number of pump pulses (top and bottom axes, respectively). The operational lifetime ($\tau_{1/2}^{ASE}$) for each case is defined as the time (or number of pump pulses), at which I_{out}^{ASE} decays to half of its initial value. Excitation was done at the same spot of the sample in air under an extreme pump of ($I_{pump} = 2500\,kW\,cm^{-2} > 20 \times I_{th-ASE}$).

2.3. Amplified Spontaneous Emission Properties

The detection in the fs-TAS experiment of stimulated emission in the same time range than spontaneous emission aims us to carry out experiments of ASE and to explore potential lasing applications. **Figure 3** shows the results of the optical (absorption and PL) and ASE experiments in polystyrene (PS) films containing 1 wt.% of **NNR-1**, **NNR-2**, and **NNR-3**. Only some data could be obtained for **NNR-4** (see Figure S4 and Table S3, Supporting Information), due to the impossibility to grow suitable films (i.e., due to the large molecular weight and the presence of many flexible alkoxy groups).[24,47–49] The ASE phenomenon is shown as a sudden increase in the output intensity (I_{out}) accompanied by a narrowing of the PL spectrum when a certain pump energy density (E_{pump}) value is exceeded, which is known as ASE threshold (E_{th-ASE}). The three investigated materials have shown ASE activity. The spectra for **NNR-n**-doped PS films (dispersed at 1 wt.%) are shown in Figure 3a and their most important optical parameters are gathered in **Table 1**. ASE peaks (λ_{ASE}) appear at 610.6 nm for **NNR-1**, 702.5 nm for **NNR-2**, and 749.9 nm for **NNR-3**, the latter representing an outstanding ASE emission in the NIR region. It is valuable to compare these findings to those reported for COPV6 (Schemes 1 and 2), which can be viewed as representative examples of highly efficient ladder-type oligomers with ASE emission. The spectral emission range of ladder-type COPVs spans from 385 to 583 nm in COPV6. In the case of the **NNR-n** compounds, a much more red-shifted portion of the spectrum (ranging from 610.5 to 749.95 nm) is achieved. To put this result in context, other nanographenes (fused polycyclic aromatic compounds expanding with 2D π–conjugation in Scheme 2 not based on the ladder type concept) with ASE emissions near 800 nm have been reported.[24,47–49]

ASE emission in the three **NNR-n** compounds occurs close to the 0-1 vibronic peak of the corresponding PL spectrum in solution. The detection of ASE in this second (0-1) vibronic peak, which is associated with a progression owing to CC stretching skeletal modes, is interesting since the high frequency associated mode allows this secondary 0-1 emission to be well separated from the main 0-0 peak, reducing the adverse effect of reabsorption in the proximity of the 0-0 peak.

Table 1. Optical and ASE properties of **NNR-n*** -doped PS films.

Sample	Wt.% [a] in PS	$\lambda_{ABS-max}$ [b] [nm]	λ_{PL-max} [c] [nm]	h [d] [nm]	λ_p [e] [nm]	$t_p[\lambda_p]$ [f] [ns]	$\alpha[\lambda_p]$ [g][x 10^3 cm^{-1}]	λ_{ASE} [h] [nm]	FWHM$_{ASE}$ [i] [nm]	E_{th} – ASE[μJ cm^{-2}]] [j]	I_{th} – ASE[kW cm^{-2}] [j]	$\tau_{1/2}^{ASE}$ [I_p] [k] (pump pulses) [kW cm^{-2}]
NNR-1	1	506/544	569	471	544	4.4	1.29	610.6	12	600	140	2.9×10^4 [2500]
	3	506/544	571	474	544	4.4	3.82	612.3	12	600	140	9×10^3 [2500]
NNR-2	1	576/625	640/699	480	625	4.5	2.40	702.5	14	70	15	$>10^5$ [2500]
	3	576/625	642/702	490	625	4.5	6.3	704.1	12	38	8	4.1×10^4 [2500]
NNR-3	1	677/744	675/741	540	662	4.6	2.88	749.9	13	29	6	$>10^5$ [2500]
	3	677/744	677/744	530	662	4.6	6.8	753.4	14	28	6	$>10^5$ [2500]

[a] Error 0.1%; [b] Peak absorption wavelengths (maximum absorption peak is underlined); [c] Peak PL wavelengths (maximum PL peak is underlined); [d] Film thickness (error ≈2%); [e] Pump wavelength for ASE and PL; [f] Pump pulse width at λ_p; [g] Absorption coefficient at λ_p (error ≈ 2%); [h] ASE wavelength (error is ±0.7 nm); [i] ASE linewidth (error is ±1 nm), defined as the full width at half maximum, FWHM, well above the threshold; [j] ASE threshold (error ≈ 20%); [k] ASE operational lifetime, characterized by the photostability half-life, $\tau_{1/2}^{ASE}$, expressed in pump pulses (error ≈20 %), obtained at pump intensities, I_p, (expressed in kW cm^{-2}) indicated in the square brackets.

The ASE thresholds, E_{th-ASE}, of the investigated NNR-based films, were determined through plots of I_{out} and linewidth (defined as the full width at half maximum, FWHM) versus pump energy density (see Figure 3b). For a given film, the E_{th-ASE} value corresponds to the pump energy density at which the FWHM reaches the midpoint value between those observed at low and high excitation density, which is approximately coincident to that at which a significant slope change in I_{out} is observed. The results for all the films are included in Table 1. For the 3 wt.% doped film, the ASE for **NNR-1** is 600 μJ cm^{-2} (140 kW cm^{-2}) which is considerably improved in the larger compounds, with values as low as 38 μJ cm^{-2} (8 kW cm^{-2}) for **NNR-2**, and 28 μJ cm^{-2} (6 kW cm^{-2}) for **NNR-3** (see Figure S5, Supporting Information for a comparison of the thresholds taking into account film absorbance at the pump wavelength). This large difference in the threshold of the **NNR-1** film with respect to the other compounds (more than an order of magnitude of difference), is likely due to a greater overlap between the **NNR-1** stimulated emission and the absorption of its excited state, with a band at 650 nm (Figure 2).

The detrimental impact on ASE of such overlap between SE and ESA has been well-documented in the literature.[49–51] It is interesting to compare these values with those reported for similar compounds.[20,26,27,52] Particularly, the E_{th-ASE}, values for **NNR-1** and **NNR-2** are similar to those obtained with highly efficient laser dyes, such as perylene orange (PDI-O), COPV6 or some blue and green emitting nanographenes (FZ2 in Scheme 2).[17] Nonetheless, it must be highlighted the very low ASE threshold of the **NNR-3** film with emission at λ_{ASE} = 749.9 nm, significantly better than those reported for other NIR emitting nanographenes, with an even shorter ASE wavelength (E_{th-ASE} = 270 μJ cm^{-2} and λ_{ASE} = 712 nm).[52] This finding of improved ASE action by enlarging the molecular size is not common, since ASE is usually deteriorated when the emission is red-shifted to the NIR. As for **NNR-3**, we have characterized both the gain and losses, crucial parameters for providing a comprehensive understanding of the ASE performance. The net gain coefficients, g_{net} (see the ESI file for further details on how these values are obtained) are illustrated in Figure 3c at several pump energy densities, E_{pump}. For instance, at E_{pump} = 55 μJ cm^{-2}, a net gain of g_{net} = 6.4 cm^{-1} is measured. Although this value is slightly lower than those of state-of-the-art dyes used in laser applications (with PLQY ≈100%), it is very good considering the low dye doping ratio in the case of **NNR-3** (1 wt.%).

Nevertheless, the g_{net} value achieved for the **NNR-3** film is in line with those measured for other PDI derivatives dispersed at similar doping rates,[53] which have been effectively utilized in various types of DFB lasers. The total loss (k) was determined from Figure 3c by extrapolating the g_{net} to E_{pump} = 0 resulting in a value, k = 4.3 cm^{-1}, which aligns closely with that of other laser dyes dispersed at a similar concentration in PS.[54] This suggests that, at this low concentration, the propagation characteristics are primarily governed by the polymer host. The ASE threshold dependence with the doping ratio in the matrix was analyzed by fabricating films with 3 wt.% of **NNR-n*** (see results in Table 1). Small variations of the ASE threshold with the weight ratio are observed; only in **NNR-2** there is barely an improvement of this figure of merit. These results suggest that some dye aggregation and/or deactivation by intermolecular interactions might occur. Therefore, DFB devices were constructed with films with 1 wt.% compound load (i.e., next section).

Furthermore, the stability and photostability of the **NNR-n** films were tested. Remarkably, the **NNR-n** films exhibit similar ASE performance after exposition to air, moisture, and ambient light for several months revealing the high stability of the samples against chemicals and photodegradation. We also performed photodegradation experiments under extreme pumping conditions (i.e., energy flow is much higher than that attained at E_{th-ASE}, in particular, E_{pump} = 2500 kW cm^{-2} > 20 E_{th-ASE}), see Figure 3d. The ASE intensity of **NNR-2** and **NNR-3**-based films is kept practically unaltered after 10^5 pump pulses, while the ASE intensity decays in **NNR-1** after 2.9 × 10^4 pump pulses. Again, the robustness to photodegradation is remarkable and in the order of the best reported for highly photostable dyes like COPVn or PDIs, which keep similar performance under excitation of two times above the threshold, while for **NNR-n** the excitation is over 100 times the threshold.[20,54,55] The corresponding ASE half-lifes, $\tau_{1/2}^{ASE}$ are collected in Table 1.

2.4. Fabrication of Distributed Feedback Lasers Based on NNR-n

The potential of these compounds for laser applications is showcased through the fabrication of DFB lasers (**Figure 4**) which exhibit lasing spanning a broad range of wavelengths, all achieved at low threshold intensities. The device architecture (inset in Figure 4b) incorporates a top-layer polymeric resonator deposited on top of the **NNR**-doped PS film. This resonator consists of a 1D relief grating created on a DCG photoresist layer by HL and followed by a dry etching process.[56]

All the DFB devices prepared have 1D gratings and operate in the second order of diffraction, that is m = 2 in the Bragg condition (Equation (1)):

$$m\lambda_{Bragg} = 2n_{eff}\Lambda \quad (1)$$

where n_{eff} is the effective index of the multilayer system, which depends on h, the grating depth (d ≈110 nm in all devices), and the refractive indexes of substrate, active film, resonator, and cover; and Λ is the grating period. In second-order DFBs, light emission occurs through perpendicular out-coupling from the device surface, via first-order diffraction, at a wavelength λ_{DFB} close to λ_{Bragg}. For light propagating in a specific waveguide mode (in the designed devices, either the fundamental transversal electric TE_0 or magnetic, TM_0) and considering a pure index grating in a separated layer (as in the present case), coupled mode theory predicts the formation of a photonic stop-band (a dip) centred at λ_{Bragg}, and lasing occurs at two wavelengths, one at each edge of the dip.[30] Therefore, Λ is adjusted to ensure that λ_{Bragg} approximately matches λ_{ASE}, where the gain is maximum, and consequently the threshold is minimised. In the case of second-order devices, only the peak emitting at the longer wavelength is observed, attributed to higher radiation losses at shorter wavelengths.[57]

The geometric and operational parameters for the different fabricated DFB devices are collected in Table 2. For each **NNR-n**, various devices, with different Λ, were prepared, all emitting at wavelengths close to λ_{ASE} (emission spectra depicted in

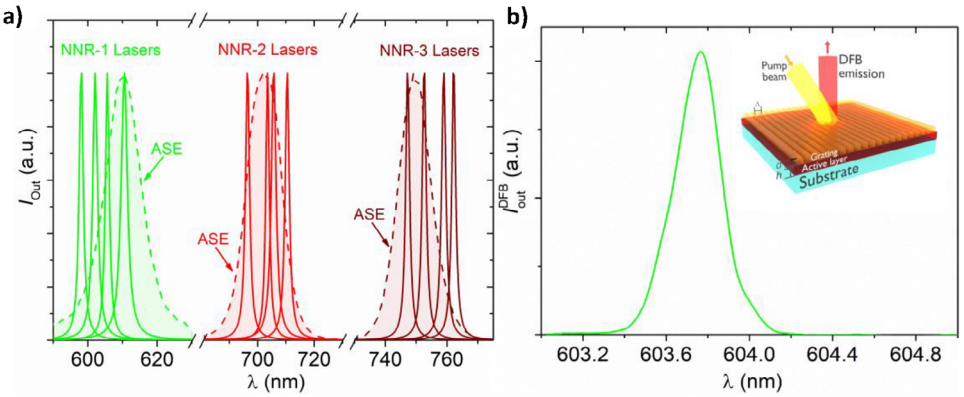

Figure 4. Distributed feedback (DFB) lasers based on NNR-n. a) Spectra of DFB lasers (solid lines) based on NNRs doped PS films (four devices for each compound with different grating periods, see **Table 2**): **NNR-1** (green), **NNR-2** (red), and **NNR-3** (maroon). Dashed lines with shaded areas correspond to the ASE spectra indicating the main laser emission region for each NNR. b) High-resolution spectrum of one the laser peak of one of the NNR1 devices on an expanded scale. The sketch of the DFB device architecture is show as an inset figure, including the excitation and collection geometries (see arrows). The device consists of a top-layer polymeric resonator with an engraved relief grating (Λ, grating period; *d*, grating depth), located over an active film (*h*, film thickness) of NNR dispersed in polystyrene (PS), deposited on top of a fused silica substrate.

Figure 4b). The four lasers created with **NNR-1** emit within the range of 603.5 to 619.3 nm, the four lasers corresponding to **NNR-2** exhibit peaks from 697.0 to 711.3 nm, and lastly, the four lasers fabricated using **NNR-3** present the most red-shifted range from 744.8 to 758.8 nm. All these peaks correspond to TE_0 waveguide modes. This was determined analyzing the polarization properties of each peak, which resulted in all cases parallel to the grating lines, which correspond to the TE_0 mode of the waveguide. The prepared waveguides also support TM_0 modes, thus laser peaks related to them also appear, whose polarization is perpendicular to the grating lines. However, because their thresholds are generally higher, often they are not detected. One of the main characteristics of the laser peaks of the prepared **NNR-n** devices is that they are very narrow (< 0.2 nm FWHM), as illustrated in Figure 4b.

The DFB threshold values (E_{th-DFB}) were determined following the same method employed for the ASE threshold determination. Similarly, upon reaching the threshold, the emission spectrum condenses into a narrow peak. Especially noteworthy are the devices fabricated with **NNR-3**, as their emission falls entirely within the NIR range, spanning from 744.8 to 758.8 nm. Additionally, all the DFB devices fabricated present a lower E_{th-DFB} than the corresponding E_{th-ASE} (see Table 2). In particular, the devices of **NNR-3** (i.e., already with the lowest E_{th-ASE}) present an exceptionally low E_{th-DFB}, of 7.5 μJ cm^{-2} (1.6 kW cm^{-2}), a result that is notable among the reported organic DFB devices and even more outstanding considering that this effect is observed in the NIR region.

3. Discussion and Conclusion

A series of benzene-perylene oligomers with rigidified ladder-type π−conjugated structures (imparted by the fourfold link between the benzene and the perylene basic units), has been studied by steady-state photophysics and transient absorption spectroscopy. According to the results, it is concluded that these

Table 2. Parameters of top-layer resonator DFB lasers based on **NNR-n***-doped (1 wt.%) PS films as active media.

Device	*h*[b] [nm]	λ_p[c] [nm]	$\alpha[\lambda_p]$[d] ($x10^3$ cm^{-1})	$t_p[\lambda_p]$[e] [ns]	Λ[f] [nm]	λ_{DFB}[g] [nm]	$E_{th}-DFB[\mu J\ cm^{-2}]$[h]	$I_{th}-DFB$[kW cm^{-2}][h]
NNR1	471	544	1.29	4.4	389.8	603.5	250	57
					392.9	608.7	220	50
	474	544	1.29	4.4	396.3	**613.3**	**300**	**68**
					399.6	619.3	310	70
NNR2	480	625	2.40	4.5	453.6	697.0	25	5.6
					456.8	**704.1**	**18**	**4.0**
	480	625	2.40	4.5	460.1	706.5	19	4.2
					463.4	711.3	22	4.8
NNR3	540	662	2.88	4.6	485.0	744.8	8.0	1.7
					488.3	749.8	7.5	1.6
	570	662	2.88	4.6	491.6	**755.7**	**9.1**	**2.0**
					494.9	758.8	9.3	2.0

[a] Error 0.1%; [b] Film thickness (error ≈2%); [c] Pump wavelength; [d] Absorption coefficient at λ_p (error ≈ 2%); [e] Pump pulse width at λ_p; [f] Grating period (error ≈ ±0.5); [g] DFB wavelength (error is ±0.7 nm); [h] DFB threshold (error ≈10%).

organic semiconductors are great candidates to extend the application of lighting into the highly desired NIR region of the electromagnetic spectrum. Special emphasis has focused on the vibronic structure of the longer **NNR-n** compounds as we prove that this is pivotal to develop emission extending toward 800 nm in **NNR-3**. This is based on the existence of high-frequency vibronic modes ≈1300 cm^{-1} (≈+ 20–30 nm at 700–750 nm) that dictate the structure of the electronic absorption and emission bands. Typically, in most π−conjugated molecules, the absorption and emission spectra are controlled by several main vibronic progressions associated with high and low frequency energy modes (i.e., ≈1300 and 300 cm^{-1}, respectively). Noticeably, in the investigated **NNR-n** family, the vibronic shapes are dictated only by high-frequency vibronic modes, which allows to extend the vibronic bands into the NIR by 20/30 nm. The absence of low-frequency vibronic modes in the electronic bands of the **NNR-n** hinders non-radiative processes that often rely on low-energy vibrations (flexing, torsional modes, etc.). In other words, the existence of large vibronic spacings in the excited states for the relevant vibrational modes that couple the ground and excited state along the $S_0 \rightarrow S_1$ and $S_1 \rightarrow S_0$ excitations could indicate a significant energy separation between the vibrational states in the excited state. This could provide reduced density of vibronic states in S_1 acting against internal conversion with the subsequent minoring of non-radiative quenching. In this way, the decrease in non-radiative processes largely increases the yield of photonic processes.

ASE has been found out in **NNR-1**, **NNR-2**, and **NNR-3** (dispersed in PS films), appearing in the 0-1 vibronic bands of the fluorescence emission, which are associated with the high frequency 1330–1350 cm^{-1} modes. This fact produces, in the case of **NNR-3**, an ASE band in the near-IR region (750 nm). Another consequence of the exciton dynamics controlled by the high frequency modes is the mitigation of non-radiative effects, thus permitting more efficient light emission even in molecules with such low band gap as those optically active in the NIR region. This is particularly the case of **NNR-3**, wherein ASE at 750 nm relates to a significantly low ASE threshold. In this regard, COPV compounds also show ASE bands in the 0-1 modes, all associated with high-frequency modes, which provide the further extension of the bands. However, given the 1D nature of COPVn, their optical bands quickly saturate with length before reaching the NIR, while the ASE thresholds decrease, effects which are not found in the **NNR-n**. On the other hand, regarding polycyclic benzenoid molecules, the elongation of the chain produces the mutation of the ASE bands from the high-frequency modes, in smaller molecules, to the low vibronic peaks, in the longer molecules. The efficient ASE emissions in the three compounds address their excellent performance shown in this work as DBF lasers. Exceptionally, **NNR-3**, with ASE in the near-IR region, allows to construct devices with responses up to 758 nm.

In contrast to the most typical way of pushing the absorptions and emission into the far red and NIR by chemical modification, we propose here an alternative mode of extending the relevant excitations into the NIR by 0.15–0.20 eV by means of high-frequency modes. Simultaneously, another benefit of such dynamic excited state effects is the intrinsic increments of the efficiency of the emissions when placed in the NIR region, which is of great relevance and beneficial for low ASE threshold materials such as **NNR-n**. We show here how the ladder-type functionalization provoking the unique rigidification of the structure of the **NNR-n** appears to be key for such findings.

Supporting Information

Supporting Information is available from the Wiley Online Library or from the author.

Acknowledgements

Financial support by the MCIN/AEI of Spain (project PID2024-157601NB-100 and RED2022-134939-T –Red de Fotovoltaica, and the Junta de Andalucía (PROYEXCEL-0328) is acknowledged. The authors also thank the Research Central Services (SCAI) and Supercomputing and Bioinnovation Center (SCBI) of the University of Málaga. J.M. M.B. wants to acknowledge the Spanish University Ministry and the European Union for his Maria Zambrano fellowship with NextGen-EU funding. M.D.-F. acknowledges the Spanish Science and Innovation Ministry for his FPI fellowship. The National Natural Science Foundation of China is acknowledged by Z.Z. (reference projects 52525306 and 22375059). J.W. acknowledges financial support from MOE Tier 2 grant (MOE-T2EP10222-0003) and A*STAR MTC IRG project (M22K2c0083). The work at the UA has been funded by the MICIU/AEI/10.13039/501100011033 (grants PID2020-119124RB-I00 and PID2023-146660OB-I00) and by the "ERDF/EU", by the "European Union" (grant PID2023-146660OB-I00). Besides, this study was part of the Advanced Materials program supported by the Spanish MCIN with funding from the European Union NextGenerationEU and by Generalitat Valenciana (grant no. MFA/2022/045).

Conflict of Interest

The authors declare no conflict of interest.

Author Contributions

M.D.F. did all spectroscopic (steady state and transient) measurements. Á.F.-P., P.G.B., J.M.V., and J.A.Q. did all experiments related to the preparation and characterization of the lasing properties. F.G.G. contributed with the experiments at low temperature. Y.W. contributed to the synthesis of the molecules. D.A. contributed with all theoretical calculations. J.M.M.-B. contributed with the interpretation of the transient absorption measurements and to the writing of the article. J.W. contributed to the realization of the investigation as well as with the writing of the article. Z.Z. provided the samples made in his lab as well as with the writing if the article. M.A.D.G. directed and interpreted all lasing properties of the molecules and contributed significantly, together with A.F.-P, to writing. J.C. conceived the work, directed the spectroscopic part and co-wrote the article.

Data Availability Statement

The data that support the findings of this study are available from the corresponding author upon reasonable request.

Keywords

amplified spontaneous emission, benzene perylene oligomers, distributed feedback lasers, ladder-type π−conjugated oligomers, spontaneous fluorescence, vibronic progressions

Received: March 11, 2025
Revised: September 15, 2025
Published online:

[1] S. Saha, S. Khamrui, R. Moi, A. Anoop, V. V. Chernyshev, D. Banerjee, K. Biradha, *ACS App. Opt. Mat.* **2023**, *1*, 2031.
[2] V. Vij, V. Bhalla, M. Kumar, *Chem. Rev.* **2016**, *116*, 9565.
[3] L. Gao, G. Ding, C. Li, Y. Wang, *Appl. Surf. Sci.* **2011**, *257*, 3039.
[4] Y. Gu, Z. Qiu, K. Müllen, *J. Am. Chem. Soc.* **2022**, *144*, 11499.
[5] J. J. Burdett, C. J. Bardeen, *Acc. Chem. Res.* **2013**, *46*, 1312.
[6] K. Zhang, X.-J. Chen, *AIP Adv.* **2018**, *8*, 025004.
[7] J. Jo, C. Chi, S. Höger, G. Wegner, D. Y. Yoon, *Chem. - Eur. J.* **2004**, *10*, 2681.
[8] L. Guo, K. F. Li, X. Zhang, K. W. Cheah, M. S. Wong, *Angew. Chem., Int. Ed.* **2016**, *128*, 10797.
[9] Z. Yang, G. Yang, S. Jiang, M. Li, W. Qiu, X. Peng, C. Shen, Y. Gan, K. Liu, D. Li, S. Su, *Adv. Opt. Mater.* **2024**, *12*, 2301711.
[10] J. Wu, *Curr. Org. Chem.* **2007**, *11*, 1220.
[11] J. M. Marin-Beloqui, K. J. Fallon, H. Bronstein, T. M. Clarke, *J. Phys. Chem. Lett.* **2019**, *10*, 3813.
[12] D. Udhayakumari, *Talanta* **2024**, *278*, 126536.
[13] A. J. C. Kuehne, M. C. Gather, *Chem. Rev.* **2016**, *116*, 12823.
[14] X. Ai, J. Mu, B. Xing, *Theranostics* **2016**, *6*, 2439.
[15] C. Chen, F. Wang, S. Wen, Q. P. Su, M. C. L. Wu, Y. Liu, B. Wang, D. Li, X. Shan, M. Kianinia, I. Aharonovich, M. Toth, S. P. Jackson, P. Xi, D. Jin, *Nat. Commun.* **2018**, *9*, 3290.
[16] R. Muñoz-Mármol, F. Gordillo, V. Bonal, J. M. Villalvilla, P. G. Boj, J. A. Quintana, A. M. Ross, G. M. Paternò, F. Scotognella, G. Lanzani, A. Derradji, J. C. Sancho-García, Y. Gu, J. Wu, J. Casado, M. A. Díaz-García, *Adv. Funct. Mater.* **2021**, *31*, 2105073.
[17] V. Bonal, R. Muñoz-Mármol, F. Gordillo Gámez, M. Morales-Vidal, J. M. Villalvilla, P. G. Boj, J. A. Quintana, Y. Gu, J. Wu, J. Casado, M. A. Díaz-García, *Nat. Commun.* **2019**, *10*, 3327.
[18] H. Meier, *Angew. Chem., Int. Ed.* **2005**, *44*, 2482.
[19] R. Englman, J. Jortner, *Mol. Phys.* **1970**, *18*, 145.
[20] X. Zhu, H. Tsuji, J. T. López Navarrete, J. Casado, E. Nakamura, *J. Am. Chem. Soc.* **2012**, *134*, 19254.
[21] P. M. Burrezo, X. Zhu, S.-F. Zhu, Q. Yan, J. T. López Navarrete, H. Tsuji, E. Nakamura, J. Casado, *J. Am. Chem. Soc.* **2015**, *137*, 3834.
[22] M. Morales-Vidal, P. G. Boj, J. M. Villalvilla, J. A. Quintana, Q. Yan, N.-T. Lin, X. Zhu, N. Ruangsupapichat, J. Casado, H. Tsuji, E. Nakamura, M. A. Díaz-García, *Nat. Comm.* **2015**, *6*, 8458.
[23] Z. Che, Y. Yu, C. Yan, S. Ge, P. Zuo, J. Wu, F. Liu, Z. Feng, L. Liao, X. Wang, *Adv. Mat.* **2025**, *37*, 2502129.
[24] C. Yan, Y. Liu, W. Yang, J. Wu, X. Wang, L. Liao, *Angew. Chem., Int. Ed.* **2022**, *61*, 202210422.
[25] L. Wang, J.-J. Wu, C. Yan, W. Yang, Z. Che, X. Xia, X. Wang, L. Liao, *Chin. Chem. Lett.* **2024**, *35*, 109365.
[26] R. Aoki, R. Komatsu, K. Goushi, M. Mamada, S. Y. Ko, J. W. Wu, V. Placide, A. D'Aléo, C. Adachi, *Adv. Opt. Mater.* **2021**, *9*, 2001947.
[27] N. R. Wallwork, A. Shukla, R. B. Roseli, I. Allison, S. K. M. McGregor, M. Coles, I. Gale, V. P. Rahane, V. Entoma, E. G. Moore, E. H. Krenske, E. B. Namdas, S. Lo, *Small* **2024**, *52*, 2406817.
[28] V. Bonal, J. M. Villalvilla, J. A. Quintana, P. G. Boj, N. Lin, S. Watanabe, K. Kazlauskas, O. Adomeniene, S. Jursenas, H. Tsuji, E. Nakamura, M. A. Díaz-García, *Adv. Opt. Mater.* **2020**, *8*, 2001153.
[29] J. A. Quintana, J. M. Villalvilla, M. Morales-Vidal, P. G. Boj, X. Zhu, N. Ruangsupapichat, H. Tsuji, E. Nakamura, M. A. Díaz-García, *Adv. Opt. Mater.* **2017**, *5*, 1700238.
[30] H. Kogelnik, C. V. Shank, *J. Appl. Phys.* **1972**, *43*, 2327.
[31] Y. Wang, Y. Huang, T. Huang, J. Zhang, T. Luo, Y. Ni, B. Li, S. Xie, Z. Zeng, *Angew. Chem., Int. Ed.* **2022**, *61*, 202200855.
[32] M. J. Frisch, G. W. Trucks, H. B. Schlegel, G. E. Scuseria, M. A. Robb, J. R. Cheeseman, G. Scalmani, V. Barone, G. A. Petersson, H. Nakatsuji, X. Li, M. Caricato, A. V. Marenich, J. Bloino, B. G. Janesko, R. Gomperts, B. Mennucci, H. P. Hratchian, J. V. Ortiz, A. F. Izmaylov, J. L. Sonnenberg, D. Williams-Young, F. Ding, F. Lipparini, F. Egidi, J. Goings, B. Peng, A. Petrone, T. Henderson, D. Ranasinghe, et al., *Gaussian 16, Revision C.01*, Gaussian, Inc, Wallingford, CT **2019**.
[33] T. Yanai, D. P. Tew, N. C. Handy, *Chem. Phys. Lett.* **2004**, *393*, 51.
[34] W. J. Hehre, K. Ditchfield, J. A. Pople, *J. Chem. Phys.* **1972**, *56*, 2257.
[35] P. C. Hariharan, J. A. Pople, *Theor. Chim. Acta* **1973**, *28*, 213.
[36] J. Cerezo, F. Santoro, *J. Comput. Chem.* **2023**, *44*, 626.
[37] F. J. Avila Ferrer, F. Santoro, *Phys. Chem. Chem. Phys.* **2012**,*14*, 13549.
[38] J. Cerezo, F. Santoro, *J. Chem. Theory Comput.* **2016**, *122*, 4970.
[39] A. Humeniuk, M. Bužancic, J. Hoche, J. Cerezo, R. Mitric, F. Santoro, V. Bonacic-Koutecký, *J. Chem. Phys.* **2020**, *152*, 054107.
[40] J. Cerezo, D. Aranda, F. J. Avila Ferrer, G. Prampolini, F. Santoro, *J. Chem. Theory Comput.* **2020**, *16*, 1215.
[41] S. Shaik, A. Shurki, D. Danovich, P. C. Hiberty, *J. Am. Chem. Soc.* **1996**, *118*, 666.
[42] Y. Haas, S. Zilberg, *J. Am. Chem. Soc.* **1995**, *117*, 5387.
[43] N. I. Nijegorodov, W. S. Downey, M. B. Danailov, *Spectrochim. Acta A Mol Biomol. Spectrosc.* **2000**, *56*, 783.
[44] Y. Yang, Z. Jiang, Y. Liu, T. Guan, Q. Zhang, C. Qin, K. Jiang, Y. Liu, *J. Phys. Chem. Lett.* **2022**, *13*, 9381.
[45] B. Schlemmer, A. Sauermoser, S. Holler, E. Zuccala, B. Ehmann, M. Reinfelds, R. C. Fischer, H. Amenitsch, J. M. Marin-Beloqui, L. Ludvíková, T. Slanina, M. Haas, T. Rath, G. Trimmel, *Chem. Eur. J.* **2023**, *29*, 202301337.
[46] W. Whitaker, I. V. Sazanovich, Y. Kwon, W. Jeon, M. S. Kwon, A. J. Orr-Ewing, *J. Phys. Chem. A* **2023**, *127*, 10775.
[47] S. M. Quintero, J. C. Mira-Martínez, Y. Zou, M. Díaz-Fernández, P. G. Boj, J. Wu, M. A. Díaz-García, J. M. Marín-Beloqui, J. Casado, *J. Mater. Chem. C Mater.* **2024**, *12*, 5239.
[48] V. T. N. Mai, A. Shukla, M. Mamada, S. Maedera, P. E. Shaw, J. Sobus, I. Allison, C. Adachi, E. B. Namdas, S.-C. Lo, *ACS Photonics* **2018**, *5*, 4447.
[49] X. Xu, R. Muñoz-Mármol, S. Vasylevskyi, A. Villa, G. Folpini, F. Scotognella, G. Maria Paternò, A. Narita, *Angew. Chem., Int. Ed.* **2023**, *62*, 202218350.
[50] S. Jarabo, M. A. Rebolledo, *Appl. Opt.* **1995**, *34*, 6158.
[51] A. Shukla, V. T. N. Mai, V. V. Divya, C. H. Suresh, M. Paul, V. Karunakaran, S. K. M. McGregor, I. Allison, K. N. Narayanan Unni, A. Ajayaghosh, E. B. Namdas, S.-C. Lo, *J. Am. Chem. Soc.* **2022**, *144*, 13499.
[52] G. M. Paternò, Q. Chen, R. Muñoz-Mármol, M. Guizzardi, V. Bonal, R. Kabe, A. J. Barker, P. G. Boj, S. Chatterjee, Y. Ie, J. M. Villalvilla, J. A. Quintana, F. Scotognella, K. Müllen, M. A. Díaz-García, A. Narita, G. Lanzani, *Mater Horiz.* **2022**, *9*, 393.
[53] E. M. Calzado, J. M. Villalvilla, P. G. Boj, J. A. Quintana, R. Gómez, J. L. Segura, M. A. Díaz García, *Appl. Opt.* **2007**, *46*, 3836.
[54] R. Muñoz-Mármol, N. Zink-Lorre, J. M. Villalvilla, P. G. Boj, J. A. Quintana, C. Vázquez, A. Anderson, M. J. Gordon, A. Sastre-Santos, F. Fernández-Lázaro, M. A. Díaz-García, *J. Phys. Chem. C* **2018**, *122*, 24896.
[55] V. Navarro-Fuster, E. M. Calzado, P. G. Boj, J. A. Quintana, J. M. Villalvilla, M. A. Díaz-García, V. Trabadelo, A. Juarros, A. Retolaza, S. Merino, *Appl. Phys. Lett.* **2010**, *97*, 171104.
[56] V. Bonal, J. A. Quintana, J. M. Villalvilla, P. G. Boj, M. A. Díaz-García, *Sci. Rep.* **2019**, *9*, 11159.
[57] R. Kazarinov, C. Henry, *IEEE J. Quantum Electron.* **1985**, *21*, 144.